



HAL
open science

Evolution of vortices created by conical diffraction in biaxial crystals versus orbital angular momentum

A Brenier

► **To cite this version:**

A Brenier. Evolution of vortices created by conical diffraction in biaxial crystals versus orbital angular momentum. *Optical Materials*, 2020, 110, pp.110504. 10.1016/j.optmat.2020.110504 . hal-02976877v2

HAL Id: hal-02976877

<https://hal.science/hal-02976877v2>

Submitted on 30 Sep 2021

HAL is a multi-disciplinary open access archive for the deposit and dissemination of scientific research documents, whether they are published or not. The documents may come from teaching and research institutions in France or abroad, or from public or private research centers.

L'archive ouverte pluridisciplinaire **HAL**, est destinée au dépôt et à la diffusion de documents scientifiques de niveau recherche, publiés ou non, émanant des établissements d'enseignement et de recherche français ou étrangers, des laboratoires publics ou privés.

Evolution of vortices created by conical diffraction in biaxial crystals versus orbital angular momentum

A. Brenier

Univ Lyon, Université Claude Bernard Lyon 1, CNRS, Institut Lumière Matière, F-69622, LYON, France

Abstract: Light states evolution versus their fractional orbital angular momentum (OAM) has been analyzed in the conical diffraction process occurring through biaxial crystals. Experimental results are provided by a non-degenerate cascade of $\text{KGd}(\text{WO}_2)_4$ and $\text{Bi}_2\text{ZnOB}_2\text{O}_6$ biaxial crystals. The continuous $0 \rightarrow 1 \rightarrow 2$ increasing of the fractional OAM in passing through integer values was operated with the help of the spin-orbit coupling in the $\text{Bi}_2\text{ZnOB}_2\text{O}_6$ crystal. The phase of the state light and its vortices were visualized by interference patterns with a reference beam. The evolution of the fractional OAM value is accompanied by a continuous evolution of pairs of vortices with opposite signs and linked by a $-\pi/+\pi$ discontinuous phase line. The phase pattern evolution around half-integer OAM is observed to be continuous. In other cases, the evolution can be interrupted by the breaking of a $-\pi/+\pi$ discontinuous phase line and a new pair of vortices with opposite charges is born.

1. Introduction

A beam going through a material is refracted and even generally doubly-refracted if the material is birefringent. This very common behaviour does not occur in the singular case of propagation along the optical axis of a biaxial crystal: W. Hamilton predicted in the nineteenth century that the refraction should be conical and a hollow cylinder should emerge [1, 2]. However, the whole optical phenomenon is quite complex and cannot be reduced to a simple propagation of rays. A

more brilliant theoretical description was obtained from plane waves decomposition [3] of the incident beam. Their recombination behind the crystal reconstitutes the conical diffraction (CD) [4] of the output beam and the richness of its structure: internal and external conical refraction both included, light dual-cone, Raman spikes and Poggendorff rings [5, 6]. Cascading several biaxial crystals leads to multiple rings and useful mode conversion. The theory for one crystal was generalised to N cascaded crystals [7]. The intensity patterns of multiple rings obtained with up to three identical crystals were experimentally exhibited [8]. In Ref. [9] an elliptical beam was launched into two cascaded crystals, reducing the intensity pattern of each circle in two lobes. Much more complex intensity patterns can be obtained inserting optical elements between the crystals. This was shown experimentally and theoretically in Ref. [10] with a $\lambda/4$ or a $\lambda/2$ plate or a linear polarizer inserted between two or more crystals. With the help of polarizers, LG_0^1 , LG_1^1 and LG_0^2 Laguerre-Gauss were exhibited in Ref. [11] with two cascaded crystals.

Interestingly, Berry et al. [12] showed that the beam emerges also with a modified orbital angular momentum (OAM). Let us recall that the OAM results of the beam linear momentum acting off-axis with respect to its centre [13]. For example, Laguerre-Gauss modes have such $l \hbar$ /photon OAM related to their $\exp(il\varphi)$ transverse phase variation. For an input field with a circular polarization, the output field after CD is a superposition of a B_0 component with a nil OAM (charge 0 component) and a B_1 component with $1 \hbar$ /photon OAM (charge 1 component). These predictions were experimentally verified in the case of the centrosymmetric $KGd(WO_2)_4$ (KGW) crystal [14] and the non-centrosymmetric (Pasteur medium) $Bi_2ZnOB_2O_6$ (BZBO) oxyborate crystal [15].

The coherent superposition of several light states with integer OAM leads to fields with average fractional OAM. This situation is mainly documented with beams emerging from spiral phase plates with fractional step height, a spatial light modulator [16-18] and superposition of appropriate LG modes with different Gouy phases [19]. The case of cascaded biaxial crystals is mainly documented for integer OAM [20-21].

The present work is devoted to the evolution of light states versus their fractional OAM, generated by cascading two different biaxial crystals optical axis oriented: KGW and BZBO (non-degenerate cascade). The phase and intensity of the coherent superposition of modes, their visualization by interference fringes and CCD camera, and their theoretical calculations by a full numerical model are presented versus the fractional OAM, including around half-integer values.

2. Experimental methods

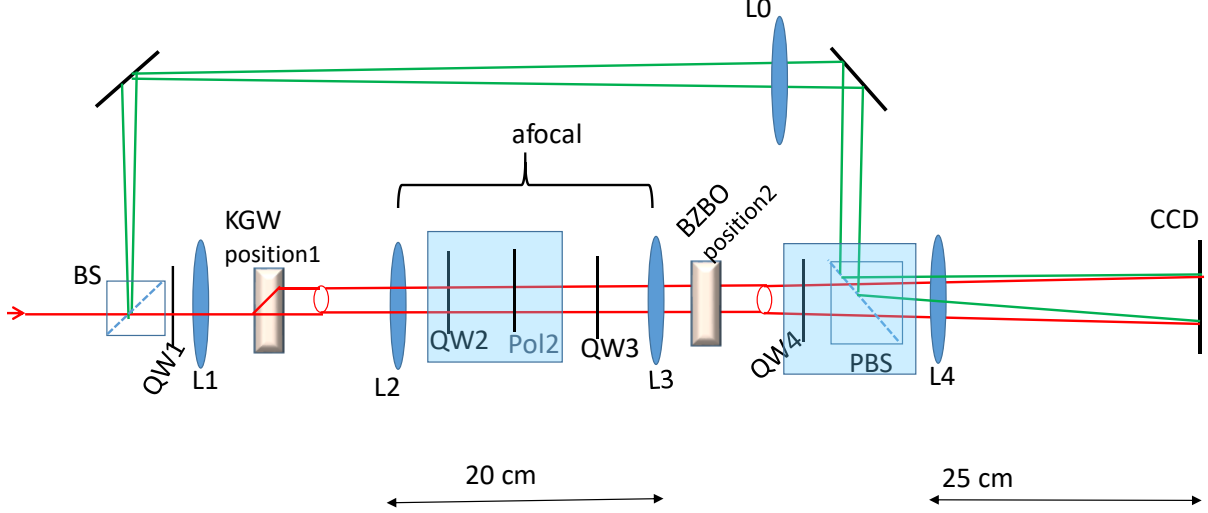


Fig. 1 Experimental set-up allowing the OAM study in the far field. The CD-field in position 1 is replicated in position 2 with -1 magnification by the L2-L3 afocal telescope. Focal length of lenses: $L0=7.5$ cm, $L1=3$ cm, $L2=L3=10$ cm, $L5=25$ cm.

A KGW ($6 \times 6 \times 3$ mm³) and a BZBO ($8 \times 6 \times 6$ mm³) crystals were used, both oriented along their optical axis. Their x-z principal plane was kept horizontal.

The linear polarized beam from a 1064 nm YAG:Nd laser was first made left circular (LC) polarized with a quarter-wave plate at the entrance of the set-up (Fig. 1). It was focused through the KGW into a $40 \mu\text{m}$ waist spot a few mm behind the sample with a doublet lens L1. In the focal plane labelled “position 1” in Fig. 1, we can observe the ring of the CD located between two axial spikes. In order to have enough space to locate several optical elements, the CD phenomenon in “position 1” was replicated without magnification but reversed 40 cm further in “position 2” with an afocal telescope. It was constituted from two $f=10$ cm focal length doublets L2 and L3, separated by twice (20 cm) their focal length. Anticipating the notations of subsection 3.1, we have the following relation between the Fourier transforms of the fields: $\hat{\mathbf{E}}(\text{position2}, k_x, k_y) = -\hat{\mathbf{E}}(\text{position1}, -k_x, -k_y)$, where the difference of the two positions is $4f$ and a phase factor omitted. In other words, the first lens performs a Fourier transform and that the second one performs the inverse Fourier transform [22]. So we obtained an exact replica of the CD phenomenon and this result is quite different of the deformation observed with a single lens in Ref. [23].

The BZBO biaxial sample was located in the position 2 and it modified the CD phenomenon. The far field resulting from the cascaded CD and propagating further position 2 was visualized through a Fourier lens L4 on the screen of a Beamage Gentec CCD camera located in the L4 focal plane. In order to visualise the phase of the near field, a reference beam was taken from the input beam with a 50/50 beam splitter and redirected with mirrors towards the CCD screen by a polarizing beam splitter near “position 2” and through the Fourier lens. The whole reference set-up is similar to a Mach-Zehnder interferometer. On the output face of the beam-splitter the two beams were a few mm separated in order to create a controlled wedge fringe pattern with the desired spatial resolution. The polarizing beam splitter reflects the vertically polarized reference beam and transmits the horizontal component of the beam under study, so their interference on the CCD is obtained through a supplementary rotated linear polarizer not shown in Fig. 1.

In Fig. 1 we can see several optical elements inserted inside the beam path: linear polarizers and quarter-wave plates, used for selecting the light states as it is detailed further.

3. Theoretical background

3.1 Beam propagation through a biaxial crystal in the Fourier space and in a circular basis

The electric field \mathbf{E} of a monochromatic beam at the input of the crystal can be decomposed in plane waves. Each of them wave inside the crystal has components on the two eigen-modes (\pm) of the refracted propagation direction and it propagates as $\exp[i(k_x x + k_y y + k_{z\pm} z)]$, with:

$$k_{z\pm} = \sqrt{k_{\pm}^2 - (k_x^2 + k_y^2)} \quad (1)$$

k_x, k_y being the transverse components of the wave-vector and k_{\pm} being the two eigen-values.

At the exit of the crystal with thickness L the emerging field $[\hat{\mathbf{E}}(L, k_x, k_y)]_{xy}$ is obtained from a linear operator $\hat{\mathbf{U}}$ acting on $[\hat{\mathbf{E}}(0, k_x, k_y)]_{xy}$:

$$\hat{\mathbf{U}} = \exp \left\{ izP \begin{bmatrix} k_{z+} & 0 \\ 0 & k_{z-} \end{bmatrix} P^{-1} \right\} \quad (2)$$

where P is the transfer matrix from the xy -frame towards the eigen-modes frame. The parabolic approximation leads to smart results for the eigen-values, the eigen-modes and the operator $\hat{\mathbf{U}}$ [3, 4]. In the present work we operated a full numerical calculation (with the Matlab package) of the $\hat{\mathbf{U}}$ operator and of any fields such as $\hat{\mathcal{Q}}$ and $\hat{\mathcal{R}}$ hereafter, with the exact refractive indices and eigenmodes as it is detailed in Ref. [15] and including birefringence and bi-anisotropy.

Moreover, for any path of length Δz in free space after the exit face of one crystal, it is necessary to multiply the field by $\exp(i\sqrt{k_0^2 - (k_x^2 + k_y^2)}\Delta z)$, k_0 being the free-space wave-vector. Of course the field in a given plane of the real space (near field, exhibited for example in Ref. [15]) is provided by the inverse Fourier transform, but in the present work we do not use this route, we work in the Fourier space (far field detected in the focal plane of the L4 Fourier lens). As it was recognized many years ago [12] waves with circular polarizations (CP) have a special role. Launching such a wave with no OAM inside a birefringent KGW crystal leads to two superimposed emerging waves \mathfrak{L} (LCP) and \mathfrak{R} (RCP) after CD in a birefringent biaxial crystal, the one with the opposite CP having its OAM modified as ± 1 , the one with the same CP having no OAM (throughout the text the OAM is expressed in \hbar /photon). The corresponding far fields $\widehat{\mathfrak{L}}$ and $\widehat{\mathfrak{R}}$ are constituted of concentric rings, they are well studied generally from reasonable approximations applied to the refractive indices and propagation eigenmodes. So, they are known to be pure states of the z-component of the OAM operator:

$$\widehat{L}_z = -i\hbar(k_x \frac{\partial}{\partial k_y} - k_y \frac{\partial}{\partial k_x}) \quad (3)$$

(Darwin result [24] restricted to the 2D monochromatic case).

Expressing the \widehat{U} operator (Eq. (2)) in a circular basis we can calculate the far field output (two LCP and RCP components) resulting from a LCP input plane wave as:

$$\begin{bmatrix} \widehat{\mathfrak{L}}_i^{(0)} \\ \widehat{\mathfrak{R}}_i^{(1)} \end{bmatrix} = \widehat{U} \begin{bmatrix} 1 \\ 0 \end{bmatrix} \quad (4)$$

and the field resulting from a RCP input plane wave as:

$$\begin{bmatrix} \widehat{\mathfrak{L}}_i^{(-1)} \\ \widehat{\mathfrak{R}}_i^{(0)} \end{bmatrix} = \widehat{U} \begin{bmatrix} 0 \\ 1 \end{bmatrix} \quad (5)$$

where the superscripts are the OAM (\widehat{L}_z eigenvalue) of the CP wave.

Then the CD through the KGW crystal labelled $i=1$ is obtained with the operator:

$$\widehat{U}_i(L, k_x, k_y) = \begin{bmatrix} \widehat{\mathfrak{L}}_i^{(0)} & \widehat{\mathfrak{L}}_i^{(-1)} \\ \widehat{\mathfrak{R}}_i^{(1)} & \widehat{\mathfrak{R}}_i^{(0)} \end{bmatrix} \quad (6)$$

Let us add that our numerical calculations lead to 0.997 instead of 1, meaning that our numerical error is about 0.3 %.

The case of the BZBO crystal, labelled $i=2$, needs a supplementary explanation. This is because this crystal is orthorhombic and acentric with point group mm2 (C_{2v}). It exhibits a natural optical activity, described by a tensor χ_a , and responsible for the rotation of a linear polarization

launched along the optical axis [15]. At 1064 nm, we measured the specific rotatory power ρ to be 0.867 rad/cm. Strictly speaking, the far fields such $\hat{\mathfrak{R}}_2^{(c)}$ are no more pure \hat{L}_z eigenstates with integer OAM. Evaluating the c-charge of a $\begin{bmatrix} \hat{\mathfrak{L}} \\ \hat{\mathfrak{R}} \end{bmatrix}$ general field in the Fourier space with the Darwin formula:

$$l_z = \frac{\mathcal{R}_e \iint [\hat{\mathfrak{L}}^* (\hat{L}_z \hat{\mathfrak{L}}) + \hat{\mathfrak{R}}^* (\hat{L}_z \hat{\mathfrak{R}})] dk_x dk_y}{\iint [|\hat{\mathfrak{L}}|^2 + |\hat{\mathfrak{R}}|^2] dk_x dk_y} \quad (7)$$

where \mathcal{R}_e means “real part”, we found $c=0.995$. This is very slightly smaller than 1, in agreement with Berry prediction about the influence of chirality on CD. But taking into account the numerical uncertainty and the closeness of c to 1, we will neglect at this step the OAM mixture and we will use operator (4) with $i=2$.

Finally, in the following sections we will calculate the spin of the field according to Darwin:

$$s_z = \frac{\iint [|\hat{\mathfrak{L}}|^2 - |\hat{\mathfrak{R}}|^2] dk_x dk_y}{\iint [|\hat{\mathfrak{L}}|^2 + |\hat{\mathfrak{R}}|^2] dk_x dk_y} \quad (8)$$

3.2 Beam with fractional orbital angular momentum

In a previous work [21] the states with increasing integer OAM (0, 1, 2) after the BC2 crystal were studied in the real space (intensity and phase). At the opposite in the present work we focus on the states with fractional OAM in the Fourier space. Their evolution is studied from the θ angle continuously varied in the $[-45^\circ, +45^\circ]$ interval.

The optical elements located after one crystal number i modify the wave polarization according to their Jones matrix in the circular basis (obtained with the help of the transfer matrix:

$$\frac{1}{\sqrt{2}} \begin{pmatrix} 1 & -i \\ 1 & i \end{pmatrix}.$$

We can see in Fig. 1 two composite elements constituted by a quarter-wave plate with its slow axis making a $\alpha = \pm 45^\circ$ angle with the x-horizontal axis, followed by a horizontal linear polarizer. They are shown inside two boxes (QW2-Pol2 and QW4-Pol3 with a polarizing beam splitter as pol3) because they are used as a whole. The Jones matrix of the box is:

$$J_{\mathfrak{R}} = \frac{1}{\sqrt{2}} \begin{bmatrix} 0 & 1 \\ 1 & 0 \end{bmatrix} \quad (9)$$

if $\alpha = +45^\circ$ and:

$$J_{\mathfrak{L}} = \frac{1}{\sqrt{2}} \begin{bmatrix} 1 & 0 \\ 1 & 0 \end{bmatrix} \quad (10)$$

if $\alpha = -45^\circ$ (α is respectively α_2 or α_4 for QW2-Pol2 box and QW4-Pol3 box).

The role of $J_{\mathfrak{R}}$ and $J_{\mathfrak{L}}$ in the experimental set-up is straightforward: $J_{\mathfrak{R}}$ projects a light state $\begin{bmatrix} \widehat{\mathfrak{R}}^{(cL)} \\ \widehat{\mathfrak{R}}^{(cR)} \end{bmatrix}$ onto a state with the charge cR of the right CP, while $J_{\mathfrak{L}}$ projects onto a state with the charge cL of the left CP. More, the two obtained states are horizontally polarized. In other words, the role of $J_{\mathfrak{R}}$ and $J_{\mathfrak{L}}$ is to select a wanted charge (the highest if the purpose is scaling the OAM).

In the following the QW2-pol2 box will always be used as a $J_{\mathfrak{R}}$ operator. The polarization of the state after this box is further modified with an additional quarter-wave plate QW3. This latter modification does not change the charge of the light state but generally, an elliptical state is obtained from an angle θ between the QW3 slow axis and the x-horizontal axis. The resulting change of the beam spin will have drastic influence on the final OAM after BC2 as it is shown in the following.

We use as input field a Gaussian beam: $\left[\widehat{G} = \widehat{G}(0) \exp\left(-\frac{w_0^2(k_x^2 + k_y^2)}{4}\right) \right]_{xy}$. With the help of Eq.

(6) for BC1 (KGW), the field state obtained after the $J_{\mathfrak{R}}$ projector and QW3 can be summarized as:

$$\begin{bmatrix} 1 \\ 0 \end{bmatrix} \widehat{G} \rightarrow \text{BC1} \rightarrow \begin{bmatrix} \widehat{\mathfrak{R}}_1^{(0)} \\ \widehat{\mathfrak{R}}_1^{(1)} \end{bmatrix} \widehat{G} \rightarrow J_{\mathfrak{R}} \rightarrow \frac{\widehat{\mathfrak{R}}_1^{(1)}}{\sqrt{2}} \begin{bmatrix} 1 \\ 1 \end{bmatrix} \widehat{G} \rightarrow \text{QW3}(\theta) \rightarrow \frac{\widehat{\mathfrak{R}}_1^{(1)}}{\sqrt{2}} \begin{bmatrix} 1 + ie^{2i\theta} \\ 1 + ie^{-2i\theta} \end{bmatrix} \widehat{G} \quad (11)$$

This is a charge 1 state whatever the θ angle. The θ angle determines the field spin which is the sum (from EQ. (8)) of a LC component $S_L(\theta)$ and a RC one $S_R(\theta)$:

$$S_L(\theta) = \frac{1 + \sin(2\theta)}{2} \quad (12)$$

$$S_R(\theta) = -\frac{1 - \sin(2\theta)}{2} \quad (13)$$

Applying Eq. (4) again the field after the BZBO=BC2 crystal was calculated with the following step:

$$\rightarrow \text{BC2} \rightarrow \frac{1}{2} \begin{bmatrix} (1 + ie^{-2i\theta}) \widehat{\mathfrak{L}}_2^{(0)} \widehat{\mathfrak{R}}_1^{(1)} + (1 + ie^{2i\theta}) \widehat{\mathfrak{L}}_2^{(-1)} \widehat{\mathfrak{R}}_1^{(1)} \\ (1 + ie^{-2i\theta}) \widehat{\mathfrak{R}}_2^{(1)} \widehat{\mathfrak{R}}_1^{(1)} + (1 + ie^{2i\theta}) \widehat{\mathfrak{R}}_2^{(0)} \widehat{\mathfrak{R}}_1^{(1)} \end{bmatrix} \widehat{\mathfrak{G}} \quad (14)$$

To take into account the influence of the afocal optics, we replaced in Eq. (14) $\widehat{\mathfrak{R}}_1^{(1)}(k_x, k_y)$ by $-\widehat{\mathfrak{R}}_1^{(1)}(-k_x, -k_y)$ in agreement with the comments in section 2. As we can see, at the exit of the BC2 crystal, the light state is a coherent superposition of several \widehat{L}_z eigenstates with integer OAM. We have selected some of them playing with the optical elements located after BC2.

The state obtained from the QW4-Pol3 box used as a $J_{\mathfrak{R}}$ operator is:

$$|J_R\rangle = \frac{1}{2\sqrt{2}} \left\{ (1 + ie^{-2i\theta}) \widehat{\mathfrak{R}}_2^{(1)} \widehat{\mathfrak{R}}_1^{(1)} + (1 + ie^{2i\theta}) \widehat{\mathfrak{R}}_2^{(0)} \widehat{\mathfrak{R}}_1^{(1)} \right\} \widehat{\mathfrak{G}} \begin{bmatrix} 1 \\ 1 \end{bmatrix} \quad (15)$$

while from the box used as a $J_{\mathfrak{Q}}$ operator it is:

$$|J_L\rangle = \frac{1}{2\sqrt{2}} \left\{ (1 + ie^{-2i\theta}) \widehat{\mathfrak{L}}_2^{(0)} \widehat{\mathfrak{R}}_1^{(1)} + (1 + ie^{2i\theta}) \widehat{\mathfrak{L}}_2^{(-1)} \widehat{\mathfrak{R}}_1^{(1)} \right\} \widehat{\mathfrak{G}} \begin{bmatrix} 1 \\ 1 \end{bmatrix} \quad (16)$$

The state obtained by fixing $\theta = 0^\circ$ and α_4 continuously varying is:

$$|\alpha_4\rangle = \frac{1+i}{4\sqrt{2}} \widehat{\mathfrak{R}}_1^{(1)} \left\{ (1 + ie^{2i\alpha_4}) (\widehat{\mathfrak{L}}_2^{(0)} + \widehat{\mathfrak{L}}_2^{(-1)}) + (1 + ie^{-2i\alpha_4}) (\widehat{\mathfrak{R}}_2^{(0)} + \widehat{\mathfrak{R}}_2^{(1)}) \right\} \widehat{\mathfrak{G}} \begin{bmatrix} 1 \\ 1 \end{bmatrix} \quad (17)$$

4. Results

The light states versus their OAM described by Eq. (15), (16) and (17) are studied in the following three subsections. Efforts were made to study the field inside the dark regions of the field intensity where the phase vortices are located. The light intensities and specially the dark region locations, measured by the CCD camera and calculated theoretically, are represented in Fig. 2. This figure will be commented simultaneously with Fig. 3, 4 and 5 in the 4.1, 4.2 and 4.3 Subsections. In particular we will explain why the two panels (d-d') and (g-g') are different despite their OAM is 1. The contrast of the interference fringes in the dark regions in Fig. 3, 4 and 5 was improved sometimes to the detriment of the bright regions.

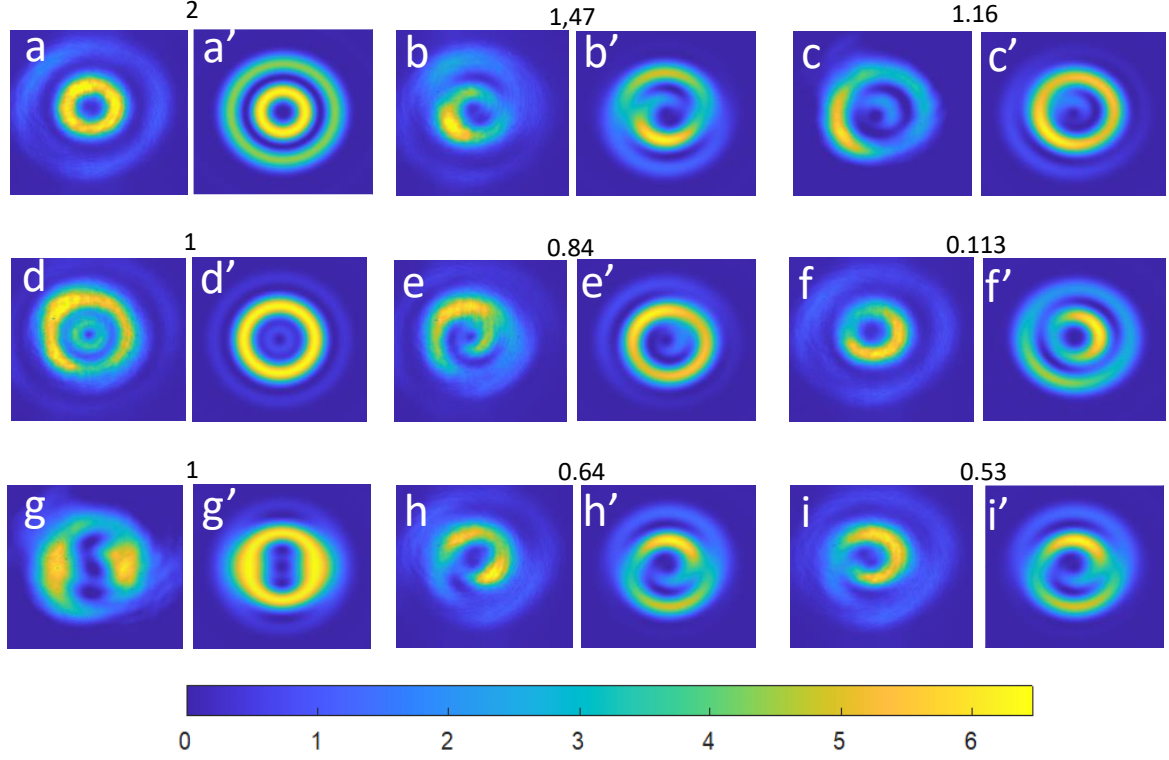


Fig. 2 Intensity patterns in the far field for various OAM (\hbar /photon). For each OAM the left picture is experimental, the right one is theoretical. The intensity scale is in arbitrary units.

4.1 Fractional OAM in the $[1, 2]$ interval

Eq. (15) shows that after the $J_{\mathfrak{R}}$ operator, the light state $|J_R\rangle$ is a coherent superposition of the two integer OAM states:

$$|1a\rangle = \hat{\mathfrak{R}}_2^{(0)} \hat{\mathfrak{R}}_1^{(1)} \hat{G} \begin{bmatrix} 1 \\ 1 \end{bmatrix}$$

$$|2\rangle = \hat{\mathfrak{R}}_2^{(1)} \hat{\mathfrak{R}}_1^{(1)} \hat{G} \begin{bmatrix} 1 \\ 1 \end{bmatrix}$$

whose charge is respectively 1 and 2. So the superposition has generally a fractional OAM in the $[1, 2]$ interval, given by the following formula obtained from inserting Eq. (15) into Eq. (7):

$$l_z = \frac{2(1+\sin(2\theta))\langle 2|2\rangle + (1-\sin(2\theta))\langle 1a|1a\rangle}{(1+\sin(2\theta))\langle 2|2\rangle + (1-\sin(2\theta))\langle 1a|1a\rangle} \quad (18)$$

with the numerical values $\langle 1a|1a \rangle = 2.83 \cdot 10^{-3} a. u.$, $\langle 2|2 \rangle = 2.49 \cdot 10^{-3} a. u.$, where we have benefited from the states orthogonality calculated to be $\langle 2|1a \rangle \cong 10^{-10} a. u.$ (which is much weaker than $\langle 2|2 \rangle$ and $\langle 1a|1a \rangle$).

Combining now Eq. (18) and (12) we can exhibit the spin-orbit coupling with the LC component of the incident state in the BC2 crystal responsible for the l_z increasing from 1:

$$l_z(\theta) = 1 + \frac{2\langle 2|2 \rangle}{(1+\sin(2\theta))\langle 2|2 \rangle + (1-\sin(2\theta))\langle 1a|1a \rangle} S_L(\theta) \quad (19)$$

where the coefficient of $S_L(\theta)$ is a fraction found numerically close to 1 (it should be exactly 1 if the eigenstates had the same modules or if $\theta = 45^\circ$).

In the extreme case $\theta = 45^\circ$ (intensity in Fig. 2 (a) and (a')), the light state is the pure OAM state $|2 \rangle$ with its OAM=2. The interference pattern with the reference beam exhibits at its centre a vortex characterized by two supplementary bright fringes located in the lower part of a circle centred on the vortex (red arrow inside Fig. 3 (a)). This corresponds to 4π rad phase variation along a path around it as the theoretical Fig. 3 (a') shows. The two $-\pi/\pi$ discontinuous phase lines near the centre in Fig. 3 (a') reveal the fact that the phase-front is helicoidal. As soon as the θ angle decreases towards 0, the light state becomes a mixing, the charge-2 vortex splits into two charge +1 vortices and l_z becomes fractional. This is shown in the case $\theta = 0$ (intensity in Fig. 2 (b) and (b')), red arrows near the middle of Fig. 3 (b) and middle of Fig. 3 (b')). The l_z value is 1.47, that is to say very close to the 1.5 half-integer value. Simultaneously a new other charge -1 vortex appears (upper red arrow in Fig. (3b)) which is linked by a bright fringe to one previous charge +1 vortex (this link is underlined by the two linked red arrows). The theoretical Fig. 3 (b') shows also the link between these two opposite signs vortices. Simultaneously another charge +1 vortex appears (bottom red arrow in Fig. 3 (b) and Fig. 3 (b')). All these vortices and their links evolve continuously up to a value of the θ angle slightly negative. Then a rearrangement occurs, shown in Fig. (3c) and (3c') for $\theta = -20^\circ$ ($l_z = 1.16$) and a new link, pointed out by the two linked red arrows, appears between two opposite charge vortices (corresponding intensity shown in Fig. 2 (c) and (c')). These two latter vortices and their link disappear in a continuous evolution (not shown in Fig. 3) when the θ angle decreases towards $\theta = -45^\circ$ ($l_z = 1$).

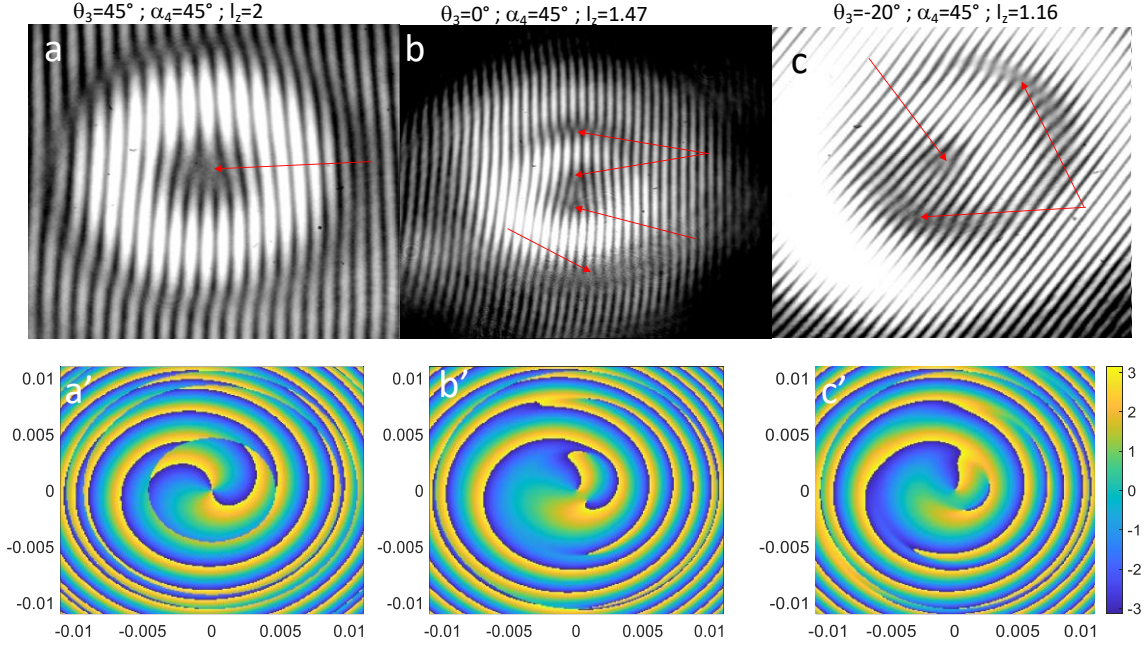


Fig. 3 Interferogram and phase pattern of the $|J_R\rangle$ state with various OAM. The red arrows point out the singularities (vortices) of the wave phase, they are paired when two vortices of opposite charges are linked by a $-\pi/\pi$ discontinuous phase lines.

4.2 Fractional OAM in the $[0, 1]$ interval

Eq. (16) shows that after the J_R operator, the light state $|J_L\rangle$ is a coherent superposition of the two integer OAM states:

$$|0\rangle = \hat{\mathcal{L}}_2^{(-1)} \hat{\mathcal{R}}_1^{(1)} \hat{\mathcal{G}} \begin{bmatrix} 1 \\ 1 \end{bmatrix}$$

$$|1b\rangle = \hat{\mathcal{L}}_2^{(0)} \hat{\mathcal{R}}_1^{(1)} \hat{\mathcal{G}} \begin{bmatrix} 1 \\ 1 \end{bmatrix}$$

whose charge is respectively 0 and 1. The resulting fractional OAM in the $[0, 1]$ interval, given by the following formula:

$$l_z = \frac{(1+\sin(2\theta))\langle 1b|1b\rangle}{(1+\sin(2\theta))\langle 1b|1b\rangle + (1-\sin(2\theta))\langle 0|0\rangle} \quad (20)$$

with the numerical values $\langle 1b|1b\rangle = 2.83 \cdot 10^{-3} a.u.$, $\langle 0|0\rangle = 2.49 \cdot 10^{-3} a.u.$, and where we have benefited from the states orthogonality calculated to be $\langle 0|1b\rangle \cong 10^{-10} a.u.$.

Combining now Eq. (20) and (13) we can exhibit the spin-orbit coupling in the BC2 crystal with the RC component of the incident state responsible for the l_z decreasing from 1:

$$l_z(\theta) = 1 + \frac{2\langle 0|0\rangle}{(1+\sin(2\theta))\langle 1b|1b\rangle+(1-\sin(2\theta))\langle 0|0\rangle} S_R(\theta) \quad (21)$$

where the coefficient of $S_R(\theta)$ is a fraction found numerically close to 1

In the case $\theta = 45^\circ$ (intensity in Fig. 2 (d) and (d')), the light state is a pure $|1b\rangle$ OAM=1 state and the interference pattern with the reference beam exhibits at its centre a vortex characterized by one supplementary bright fringe located in the lower part of a circle centred on the vortex (red arrow inside Fig. 4 (a)). This corresponds to 2π rad phase variation along a path around it as the theoretical Fig. 4 (a') shows. The $-\pi/+\pi$ discontinuous phase line near the centre in Fig. 4 (a') reveal the fact that the phase-front is helicoidal. As soon as the θ angle decreases towards 0, this $-\pi/+\pi$ discontinuous phase line breaks and two new vortices with opposite charges are born near the centre. This is shown in Fig. 4 (b) and (b') (red arrows) corresponding to $\theta = +20^\circ$ ($l_z = 0.84$, intensity shown in Fig. 2 (e) and (e')). The new -1 charge vortex is linked with + 1 charge original vortex (pointed out by the two linked red arrows). Then a continuous evolution of this structure is observed when θ and l_z decrease. This is shown in Fig. 5 (c) and (c') for $\theta = 0$ and $l_z = 0.53$ (intensity represented in Fig. 2 (i) and (i')). The values $\theta = -20^\circ$ and $l_z = 0.113$ lead to Fig. 4 (c) and (c') (here the experimental resolution is not sufficient to distinguish the two opposite charge vortices in the centre), the intensity being shown in Fig. 2 (f) and (f')); all the vortices disappear for $\theta = -45^\circ$ and $l_z = 0$ (this case is not shown).

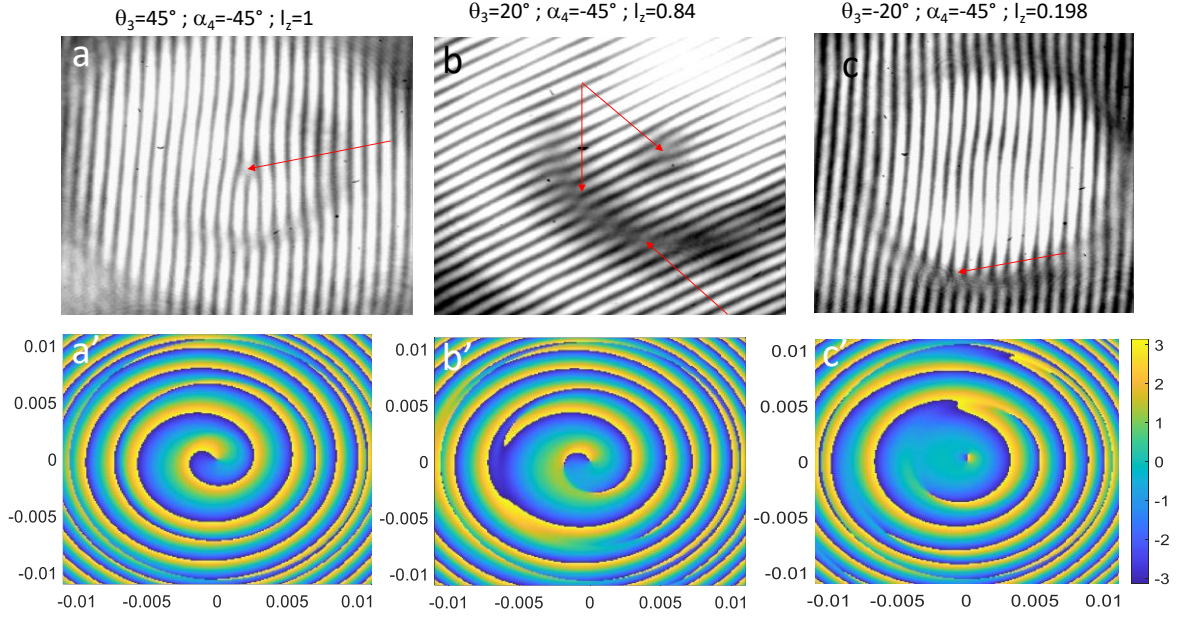


Fig. 4 Interferogram and phase pattern of the $|J_L\rangle$ state with various OAM. The red arrows point out the singularities (vortices) of the wave phase, they are paired when two vortices of opposite charges are linked by a $-\pi/\pi$ discontinuous phase lines.

4.3 Composite states with total OAM around $1 \hbar/\text{photon}$

Eq. (17) shows that the $|\alpha_4\rangle$ state is a superposition of the $|0\rangle$, $|1a\rangle$, $|1b\rangle$ and $|2\rangle$ states. The resulting fractional OAM is given by the following formula:

$$\begin{aligned}
 l_z &= \\
 &= \frac{2(1 + \sin(2\alpha_4)) \langle 2|2\rangle + (1 + \sin(2\alpha_4)) \langle 1a|1a\rangle + (1 - \sin(2\alpha_4)) \langle 1b|1b\rangle}{(1 + \sin(2\alpha_4)) \langle 2|2\rangle + (1 + \sin(2\alpha_4)) \langle 1a|1a\rangle + (1 - \sin(2\alpha_4)) \langle 1b|1b\rangle + (1 - \sin(2\alpha_4)) \langle 0|0\rangle}
 \end{aligned}
 \tag{22}$$

where we have used $\langle 1a|1b\rangle \cong 10^{-5} a.u.$, $\langle 2|1b\rangle \cong 10^{-10} a.u.$, $\langle 0|1a\rangle \cong 10^{-11}$, $\langle 0|2\rangle \cong 10^{-11} a.u.$

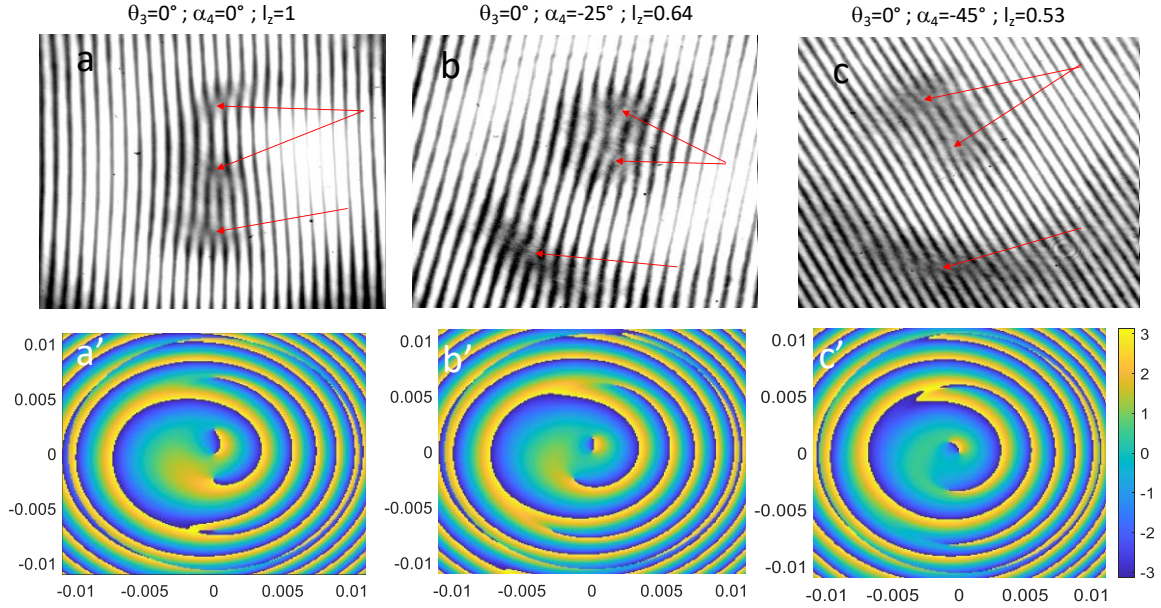


Fig. 5 Interferogram and phase pattern of the $|\alpha_4\rangle$ state with various OAM. The red arrows point out the singularities (vortices) of the wave phase, they are paired when two vortices of opposite charges are linked by a $-\pi/+\pi$ discontinuous phase lines.

Let us start with the state $|\alpha_4 = 0\rangle$ obtained with the $\alpha_4 = 0^\circ$ angle. We have $l_z = 1$ but despite that this value is integer it is an average over four pure states, the state intensity (Fig. 2 (g) and g')) has not a circular symmetry unlike the $|1b\rangle$ eigen-state (Fig. 2 (d) and d')). This is of course because this $|\alpha_4 = 0\rangle$ state is not a pure state of OAM but is a coherent superposition of four eigen-modes. This intensity vanishes in three points where we expect vortices. This is what we found in Fig 5 (a) and (a'). Two opposite charge vortices are linked by a $-\pi/+\pi$ discontinuous phase line (linked red arrows). When decreasing the α_4 angle, the intensity, interference pattern and phase evolves continuously. This is shown for the state $|\alpha_4 = -25^\circ\rangle$ ($l_z = 0.64$, Fig 2 (h) and (h'), Fig 5 (b) and (b')), and for the state $|\alpha_4 = -45^\circ\rangle$ ($l_z = 0.53$, Fig 2 (i) and (i'), Fig 5 (c) and (c')).

4.4 Discussion of the results

We have shown that a pair of vortices of integer charge of the same sign (+1) is born when lowering from $l_z = 2$ the OAM of the light state. We have shown that the continuous evolution of the phase pattern going with the l_z evolution is sometimes interrupted by the breaking of a -

$\pi/+\pi$ discontinuous phase line linking two existing opposite charge vortices. In this case a new pair of vortices with opposite charges is born. If we inspect the case of the phase pattern evolution around half-integer OAM, that is to say around 1.5 (Fig. 3 (b) and (b')) and 0.5 (Fig. 5 (c) and (c')), we observe a continuous evolution and not a specific pattern or a sudden transition. This is in contrast with the change of vortex topology reported in previous works concerning the phase pattern of fields created by spiral phase plates with fractional step height or spatial light modulator. In these cases, for half-integer phase steps, a chain of additional vortices with alternating charge is observed experimentally and theoretically in the region of low intensity [16-18].

5. Conclusions

The mechanisms leading to the evolution of light states versus their fractional OAM from a CP Gaussian beam with no OAM have been pointed out in the cascaded CD process. Experimental results are provided by a non-degenerate cascade of two different KGW and BZBO biaxial crystals. The $0 \rightarrow 1 \rightarrow 2$ increasing of the OAM in passing through fractional values was operated with the help of the spin-orbit coupling in the BZBO crystal. The phase of the state light and its vortices were visualized by interference patterns with a reference beam. The evolution of the fractional OAM value is accompanied by a continuous evolution of pairs of vortices with opposite signs and linked by a $-\pi/+\pi$ discontinuous phase line. The phase pattern evolution around half-integer OAM, that is to say around 1.5 and 0.5, is observed to be continuous and not with a specific or a sudden behaviour. In other cases, the evolution can be interrupted by the breaking of a $-\pi/+\pi$ discontinuous phase line and a new pair of vortices with opposite charges is born. All the experimental patterns (intensity, phase, OAM) are quite well described by a full numerical mode exhibited in the Fourier space.

Our study is devoted to fractional OAM generated by the peculiar mechanism of CD, but other devices have proved their efficiency in this field, such as spiral phase plates or spatial light modulators. Fractional OAM can correspond to a superposition of a lot of eigenstates instead of only two for polarization. So applications in quantum communications and entanglements of photons are conceivable [25].

Acknowledgments

We thank A. Majchrowski and E. Michalski for providing the BZBO sample.

References

1. L. Landau and E. Lifschitz, *Electrodynamique des milieux continus*, Ed. Mir Moscou 1969.
2. M. Born, E. Wolf, A. B. Bhatia, *Principles of optics: electromagnetic theory of propagation, interference and diffraction of light*, 7th ed. Cambridge University Press, 1999.
3. A. M. Belskii and A. P. Khapalyuk, “Internal conical refraction of bounded light beams in biaxial crystals”, *Opt. Spectrosc. (USSR)*, **44**, 436-439 (1978).
4. M. V. Berry, “Conical diffraction asymptotics: fine structure of Poggendorff rings and axial spike”, *J. Opt. A: Pure Appl. Opt.* **6**, 289-230 (2004).
5. G. S. Sokolovskii, D. J. Carnegie, T. K. Kalkandjiev, and E. U. Rafailov, “Conical refraction: New observations and a dual cone model”, *Opt. Exp.* **21** n°9, 11125 (2013).
6. A. Turpin, Yu. Loiko, T. K. Kalkandjiev, H. Tomizawa, and J. Mompart, “On the dual-cone nature of the conical “refraction phenomenon”, *Opt. Lett.* **40** n°8 1639-1642 (2015).
7. M. V. Berry, “Conical diffraction from an N-crystal cascade”, *J. Opt.* **12**, 075704 (8pp) (2010).
8. A. Turpin, Y. V. Loiko, T. K. Kalkandjiev, and J. Mompart, “Multiple rings formation in cascaded conical refraction”, *Opt. Lett.* **38** n°9, 1455-1457 (2013).
9. A. Turpin, Y. V. Loiko, T. K. Kalkandjiev, and J. Mompart, “Light propagation in biaxial crystals”, *J. Opt.* **17**, 065603 (6pp) (2015).
10. S. Mohammadou, B. Mohamadou and G. Montemezzani, “Complex beam shaping by cascaded conical diffraction with intercalated polarization transforming elements”, *Opt. Exp.* **25** n°21, 25392-25406 (2017).
11. V. Peet, “Biaxial crystal as a versatile mode converter”, *J. Opt.* **12** 095706 (4pp) (2010).
12. M. V. Berry, M. R. Jeffrey, and M. Mansuripur, “Orbital and spin angular momentum in conical diffraction”, *J. Opt. A: pure Appl. Opt.* **7**, 685-690 (2005).
13. M. J. Padgett, “Orbital angular momentum 25 years on”, *Opt. Exp.*, **25** (10), 11265-11274 (2017).

14. D. P. O'Dwyer, C. F. Phelan, Y. P. Rakovich, P. R. Eastham, J. G. Lunney, and J. F. Donegan, "Generation of continuously tunable fractional optical angular momentum using internal conical diffraction", *Opt. Express*, **18** (16), 16480-16485 (2010).
15. A. Brenier, A. Majchrowski and E. Michalski, "Light propagation properties of the $\text{Bi}_2\text{ZnOB}_2\text{O}_6$ acentric biaxial crystal: angular orbital momentum from conical diffraction", *Opt. Mat.* **91**, 286-291 (2019).
16. M. V. Berry, "Optical vortices evolving from helicoidal integer and fractional phase steps", *J. opt. A: pure Appl. Opt.* **6**, 259-268 (2004).
17. J. Leach, E. Yao and M. J. Padgett, "Observation of the vortex structure of a non-integer vortex beam", *New J. Phys.*, **6**, 71 (2004).
18. J. B. Götte, S. Franke-Arnold, R. Zambrini, and S. M. Barnett, "Quantum formulation of fractional orbital angular momentum", *J. Mod. Opt.*, **54** n°12, 1723-1738 (2007).
19. J.B. Götte, K. O'Holleran, D. Preece, F. Flossmann, S. Franke-Arnold, S. M. Barnett and M. J. Padgett, "Light beams with fractional orbital angular momentum and their vortex structure", **16** n°2, 993 (2008).
20. E Jalviste, V Palm and V Peet, "Vortex light beams in a degenerate two-crystal cascade conical refraction," *J. Opt.* **20** 015601 (2018).
21. A. Brenier, A. Majchrowski and E. Michalski, "Some aspects of scaling the orbital angular momentum of light with conical diffraction", *Optik*, to be published.
22. "Fundamental of fluorescence microscopy", by Partha Pratim Mondal and Alberto Diaspro, Springer (2014). ISBN 978-94-007-7544-2.
23. E. Jalviste, V. Palm, and V. Peet, "Conically refracted Gaussian beam transformed by a lens", *J. Modern Optics*, **67**, n° 3, 252-260 (2020).
24. C. G. Darwin, "Note on the theory of radiation", *Proc. R. Soc. Lond., A Contain. Pap. Math. Phys. Character.* **136** (829), 36-52 (1932).
25. S. S. R. Oemrawsingh, A. Aiello, E. R. Eliel, G. Nienhaus, and J. P. Woerdman, "How to observe High-Dimensional Two-Photon Entanglement with Only Two Detectors," *Physical Review Letters* **92**, 217901 (2004).

Figure captions

1. Experimental set-up allowing the OAM study in the far field. The CD-field in position 1 is replicated in position 2 with -1 magnification by the L2-L3 afocal telescope.

2. Intensity patterns in the far field for various OAM. For each OAM the left picture is experimental, the right one is theoretical. The intensity scale is in arbitrary units.
3. Interferogram and phase pattern of the $|J_R\rangle$ state with various OAM. The red arrows point out the singularities (vortices) of the wave phase, they are paired when two vortices of opposite charges are linked by a $-\pi/+\pi$ discontinuous phase lines.
4. Interferogram and phase pattern of the $|J_L\rangle$ state with various OAM. The red arrows point out the singularities (vortices) of the wave phase, they are paired when two vortices of opposite charges are linked by a $-\pi/+\pi$ discontinuous phase lines.
5. Interferogram and phase pattern of the $|\alpha_4\rangle$ state with various OAM. The red arrows point out the singularities (vortices) of the wave phase, they are paired when two vortices of opposite charges are linked by a $-\pi/+\pi$ discontinuous phase lines.